Soft Matter

PAPER

View Article Online
View Journal

Cite this: DOI: 10.1039/c6sm00400h

Reversible, voltage-activated formation of biomimetic membranes between triblock copolymer-coated aqueous droplets in good solvents†

Nima Tamaddoni,[a] Graham Taylor,[a] Trevor Hepburn,[a] S. Michael Kilbey II[b] and Stephen A. Sarles*[a]

Received 17th February 2016,
Accepted 9th May 2016

DOI: 10.1039/c6sm00400h

www.rsc.org/softmatter

Biomimetic membranes assembled from block copolymers attract considerable interest because they exhibit greater stability and longetivity compared to lipid bilayers, and some enable the reconstitution of functional transmembrane biomolecules. Yet to-date, block copolymer membranes have not been achieved using the droplet interface bilayer (DIB) method, which uniquely allows assembling single- and multi-membrane networks between water droplets in oil. Herein, we investigate the formation of poly(ethylene oxide)-*b*-poly(dimethyl siloxane)-*b*-poly(ethylene oxide) triblock copolymer-stabilized interfaces (CSIs) between polymer-coated aqueous droplets in solutions comprising combinations of decane, hexadecane and AR20 silicone oil. We demonstrate that triblock-coated droplets do not spontaneously adhere in these oils because all are thermodynamically good solvents for the hydrophobic PDMS middle block. However, thinned planar membranes are reversibly formed at the interface between droplets upon the application of a sufficient transmembrane voltage, which removes excess solvent from between droplets through electrocompression. At applied voltages above the threshold required to initiate membrane thinning, electrowetting causes the area of the CSI between droplets to increase while thickness remains constant; the CSI electrowetting response is similar to that encountered with lipid-based DIBs. In combination, these results reveal that stable membranes can be assembled in a manner that is completely reversible when an external pressure is used to overcome a barrier to adhesion caused by solvent–chain interactions, and they demonstrate new capability for connecting and disconnecting aqueous droplets *via* polymer-stabilized membranes.

1 Introduction

Biomimetic membranes comprised of amphiphilic phospholipids or polymers permit scientists to study a wide variety of processes that occur at or across cellular membranes. However, due to the fragility and short lifetimes (minutes to days) of phospholipid bilayers,[1] scientists have aimed to create more robust membranes using polymerizable species, including phospholipids[2–6] or polymers,[4,7–10] and they have also looked to un-polymerized block copolymers[11–16] that mimic the structure and amphiphilicity of lipids found in cellular membranes. Like lipids, amphiphilic block copolymers are known to self-assemble spontaneously into planar membranes, spherical vesicles called polymersomes, or rod-like structures in water,[17–19] and yet they exhibit greater mechanical and chemical stability than lipids.[14,15,20] In addition to a class of molecules called Janus dendrimers,[19] diblock and triblock copolymers are the most commonly used types of amphiphilic polymers to assemble biomimetic membranes. Diblock copolymers (*i.e.* those with an AB organization) consist of one hydrophilic polymer group attached to a hydrophobic group. With this architecture, diblock copolymers such as poly(etheylene oxide)-*b*-poly(ethylene ethylene) assemble to form 2-leaflet bilayer membranes in water, similar to the organization of phospholipids in lipid bilayers.[17] Unlike diblocks, triblock architectures consisting of, for example, ABA or ABC block copolymers having hydrophilic end groups and a hydrophobic middle block can span the full thickness of the membrane they create.[13,21]

In recent years, several groups have used a specific ABA-format triblock copolymer consisting of hydrophilic poly(methyloxazoline) (PMOXA) end blocks and a hydrophobic poly(dimethyl siloxane) (PDMS) middle block.[10,12–14,16] Notably, PMOXA-*b*-PDMS-*b*-PMOXA membranes exhibit greater stability than lipid membranes[16] and

[a] Dept. of Mech., Aero. and Biomed. Engr., 1512 Middle Dr. 414 Dougherty Hall, University of Tennessee, Knoxville, TN 37996, USA. E-mail: ssarles@utk.edu
[b] Depts. of Chemistry and Chemical & Biomolecular Engineering, University of Tennessee, Knoxville, TN 37996, USA

† Electronic supplementary information (ESI) available. See DOI: 10.1039/c6sm00400h

they retain the ability to reconstitute functional protein channels and pores[12,16,22] due to the elastic, fluid nature of the PDMS block that permits the hydrophobic interior to accommodate transmembrane proteins of varying lengths.[21,23]

Planar freestanding copolymer membranes can be formed by painting a mixture of copolymer and organic solvent across the aperture of a solid support in water[12,13] *via* the methods pioneered for forming black lipid membranes (BLMs).[24–26] While this approach enables the assembly of a functional planar membrane, significant skill is required to initiate membrane thinning and this approach yields only one membrane per experiment. In contrast, droplet interface bilayers (DIBs) are planar bilayer membranes formed between lipid-coated water droplets immersed in oil.[27–29] The DIB approach for membrane assembly is straightforward, allows for independent control of droplet and leaflet compositions, and uniquely enables the construction of multiple membrane networks, which have been shown to enable collective functionality,[28,30–32] simply by adjoining more than two droplets. Thus, the ability to construct durable block copolymer membranes using the DIB approach could be used to develop new types of robust, compartmentalized materials for sensing, actuation, and energy harvesting. However, DIBs to-date have only been formed with phospholipids[33] or single-tailed amphiphilic surfactants,[34] for which it is known that the structures and sizes of these surfactant molecules play important roles in adhesion properties of the membranes formed between droplets.[35–38]

Spontaneous adhesion between surfactant-encased droplets and stabilization against coalescence, as observed with DIBs, are the result of a combination of intermolecular forces between surfactant (*i.e.* solute) and solvent molecules acting in the region between droplets.[39] The term poor solvent describes a solvent where solvent–solvent or solute–solute contacts are preferred, rather than solute–solvent interactions; on the other hand, a good solvent is one in which solute–solvent interactions are more favorable than solute–solute interactions or solvent–solvent interactions. As a result, the portion of a surfactant (*e.g.* phospholipid or polymer chain) in a good solvent expands to maximize segment–solvent contacts, whereas it collapses to minimize these unfavorable interactions in poor solvent.

Adhesion between surfactant-coated water droplets is favored when the surrounding oil is a poor solvent for the hydrophobic region of the surfactant,[36,39] which leads to the spontaneous exclusion of excess solvent from between droplets to form a solvent-free region. Entropic in nature,[40] this exclusion generates an osmotic pressure that drives the droplets together (in addition to van der Waals attractive forces) to the point where short-range repulsive forces (steric in origin) between opposing surfactant monolayers stabilize adhesion and prevent coalescence. On the other hand, when the solvent is a good solvent for the hydrophobic coronae of the surfactant-coated water droplets, excluded volume interactions between surfactant tails and solvent molecules sterically stabilizes the droplets, preventing spontaneous solvent exclusion and droplet coalescence.[36]

In this work we present the formation and characterization of fully reversible, voltage-activated copolymer stabilized droplet interfaces—which we refer to as copolymer stabilized interfaces (CSIs)—assembled between aqueous droplets coated in a monolayer of triblock copolymer molecules. The ABA triblock copolymer used in this work consists of poly(ethylene oxide) (PEO) end groups with a poly(dimethylsiloxane) (PDMS) middle group. Our results show that unlike prior studies,[12,16] which demonstrated spontaneous thinning of planar triblock membranes in the presence of a poor organic solvent for the copolymer hydrophobic block, the use of PEO-*b*-PDMS-*b*-PEO-coated droplets immersed in good solvents for the middle block does not result in spontaneous membrane thinning and droplet adhesion. However, stable droplet adhesion and film formation is achieved when a voltage-induced compression is used to drive excess solvent from the hydrophobic regions of opposing triblock monolayers. Unlike spontaneous droplet adhesion, voltage-induced thinning is fully reversible: removing the applied voltage allows the droplets to completely separate as solvent returns to the region between droplets.

The following sections present our study of the mechanism of reversible CSI formation between water droplets placed in various good solvents. Specifically, we perform experiments with the same copolymer dispersed in the organic solvents to investigate the role of solvent quality on voltage-driven exclusion and the resulting properties of the interface. In each solvent, we determine the minimum voltage required to initiate membrane thinning, and we utilize techniques developed recently by our group with lipid-based DIBs,[41] to measure the specific capacitance and electrowetting response, which allow us to then determine the hydrophobic thickness and lateral tension of the CSI, respectively. These data allow us to investigate structural differences between lipid-based DIBs and CSIs, and our results show that planar copolymer membranes are considerably thicker than lipid DIBs due to solvent retention and polymer midblock length. Additionally, we observe that CSIs exhibit increased resistance to rupture during physical perturbation and significantly higher rupture potentials compared to DIBs. Simultaneously, CSIs also exhibit similar magnitudes of membrane resistance to ion transport as lipid bilayers even though they can exist in a significantly lower tension state when formed in a silicone oil-based solvent. Thus, the ability to prevent coalescence/mixing between aqueous volumes and be reversibly connected and disconnected with voltage provides a new approach for membrane-based smart materials and reconfigurable droplet-based assays.

2 Materials and methods

Five oil compositions are used in this study: *n*-decane, *n*-hexadecane, AR20 silicone oil, a 3 : 1 (v : v) mixture of hexadecane and AR20, and a 1 : 1 (v : v) mixture of hexadecane and AR20. All solvents, sodium chloride (NaCl), 3-(*N*-morpholino)-propane-sulfonic acid (MOPS), sodium hydroxide (NaOH), and agarose (A9539) are acquired from Sigma Aldrich. PEO-*b*-PDMS-*b*-PEO (2 kDa-*b*-2 kDa-*b*-2 kDa, P7300-EODMSEO) triblock copolymer is obtained from Polymer Source Inc. 1,2-Diphytanoyl-*sn-glycero*-3-phosphocholine (DPhPC) phopspholipid is obtained in powder form from Avanti Polar Lipids, Inc.

Copolymer-stabilized droplet interfaces are created between adjacent 200 nL droplets of aqueous buffer placed in a copolymer–oil mixture or using the droplet-on-hydrogel bilayer method[42–44] for forming a gel-supported CSI (see Fig. S1 in ESI† for additional details). For each oil type, PEO-*b*-PDMS-*b*-PEO triblock is incorporated into the oil at a concentration of 4 mg mL^{-1}, vortexed, and then stirred on a magnetic hot plate at a temperature of >60 °C to facilitate complete dissolution of the polymer. The application of heat ensures that the PEO end-blocks remain above their transition temperature (~ 30 °C), as evidenced by obtaining a clear, homogeneous polymer–oil mixture. For comparison, DPhPC DIBs are formed in hexadecane between droplets containing 2 mg mL^{-1} unilamellar DPhPC liposomes (~ 100 nm) in aqueous buffer prepared *via* extrusion as described elsewhere.[45] The aqueous buffer used in CSI and DIB experiments is 100 mM NaCl, 10 mM MOPS, balanced to pH 7.4 *via* titration with an identical solution supplemented with 0.5 M NaOH. Buffer pH is verified using a Fisher Scientific Accumet pH probe. Liposome solutions are stored at 4 °C and are used within 2–3 weeks of preparation. Liposome-free aqueous buffer and polymer–oil solutions are stored at room temperature (23 °C), and polymer–oil solutions are reheated before tests to ensure complete dispersion of polymer in the oil phase. Note that only reported values of rupture potential for DPhPC DIBs in hexadecane are measured herein. All other reported values of DPhPC DIBs, including specific capacitance, thickness, contact angle, and monolayer and bilayer tensions, are sourced from prior studies by our group[41,46] that contained higher numbers of trials. All DIB and CSI tests are performed at room temperature.

Electrical measurements and optical imaging are used collectively to assess adhesive interfaces between lipid- and copolymer-coated aqueous volumes in oil. The application of voltage and measurement of current across CSIs and DIBs are made using wire-type silver/silver chloride (Ag/AgCl) electrodes. Electrodes for DIB measurements are ball-ended as described elsewhere,[28] whereas those for most CSI measurements lack a ball-ended tip and hydrogel coating, since these features complicate insertion of electrodes into polymer-encased droplets where the monolayer forms rapidly. In these experiments positive current represents flow of electrons into the headstage, and measurements are performed only at positive biases due to symmetric membrane compositions in all tests. Droplet positions are controlled manually *via* the electrodes; each electrode is attached to a 3-axis micromanipulator (KITE-R, World Precision Instruments). An AxoPatch200B and Digidata 1440A (Molecular Devices) are used to measure the square-wave current induced by a 10 mV, 10 Hz triangular voltage waveform generated by an Agilent 33210A function generator. Measurements of interfacial current are performed with grounded shielding placed near the positive electrode to minimize electromagnetic interference, and all measurements are sampled at 20 kHz and low-pass filtered with a 4-pole Bessel filter at 1 kHz. Side-by-side droplet pairs and droplets on a polymer-coated hydrogel surface are viewed through a 4× objective lens on an Olympus IX51 inverted microscope. Images are acquired with a QI Click CCD camera controlled using μManager 1.4.14 software.[47] Adhesive droplet images are post-processed in MATLAB to extract bilayer area for determining specific capacitance and contact angle for measuring interfacial tension and free energy.

3 Results

3.1 Voltage-induced adhesion of triblock-coated droplets placed in a good solvent

CSIs and DIBs between adjacent aqueous droplets are prepared using a similar procedure with only very minor differences. In both CSI and DIB cases, aqueous droplets are pipetted into a less-dense nonpolar solvent and allowed to incubate for a short period of time (<30 s for droplets in copolymer–oil mixtures *versus* 2–5 min for liposome droplets in oil[45]) to allow the amphiphiles time to self-assemble into monomolecular layers at the water–oil interfaces. Each adsorbed copolymer molecule is believed to be arranged in a looped configuration, *i.e.*, with both hydrophilic endblocks in water and the hydrophobic midblock looping out into the oil. However, once droplets are brought into contact, the two systems show significant differences. Lipid-coated droplets (Fig. 1a) spontaneously adhere upon the exclusion of excess solvent from between opposing lipid monolayers, as reported in the extensive literature on DIBs.[29] Spontaneous thinning and subsequent growth of the lipid bilayer increases the interfacial electrical capacitance which results in a measurable increase in the amplitude of the squarewave current (Fig. 1a). We also observe a brighter, planar connection between adhered droplets (right inset) that is different from what is seen in adjacent, but disconnected droplets prior to the capacitive current increase (left inset). A 10 mV amplitude triangular voltage waveform is applied continuously to induce the squarewave current necessary for measuring interfacial capacitance, however, it is important to note that adhesion between lipid-coated droplets in hexadecane occurs even in the absence of electrodes and applied voltage. In contrast, PEO-*b*-PDMS-*b*-PEO-coated droplets in a 1 : 1 (v : v) mixture of hexadecane and AR20 silicone oil (as used elsewhere[48] to minimize density differences between the aqueous and organic phase) do not adhere spontaneously when placed in contact. The same result also occurs when aqueous droplets are placed in pure decane, hexadecane, or silicone oil.

Applied voltage can be used to expedite bilayer thinning in lipid-based DIBs. Therefore a voltage difference is applied between non-adhesive copolymer-coated droplets in 1 : 1 hexadecane : AR20 oil to see if adhesion can be also obtained for this system. The leftmost section of the current trace in Fig. 1b corresponds to separated droplets (see left inset image) despite the application of 150 mV (note, voltage was increased incrementally to this level). The background capacitive current in Fig. 1b is slightly larger than in Fig. 1a due to higher electrical noise during this experiment. In the next section of Fig. 1b (middle inset), increasing the voltage from 150 mV to 200 mV results in a sudden significant increase in the amplitude of the squarewave current response. Images obtained simultaneously show that there is a visible interface to

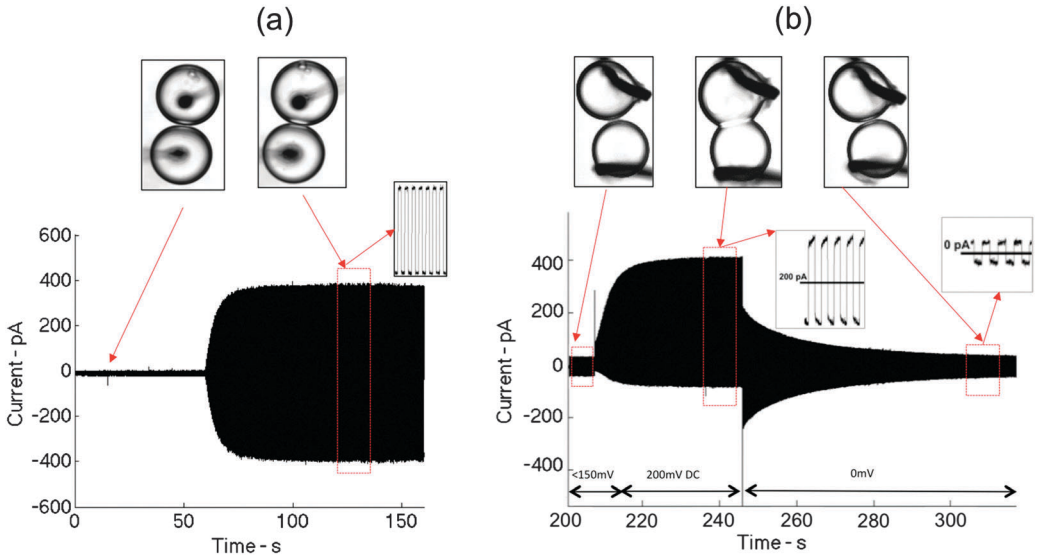

Fig. 1 (a) Spontaneous thinning of a DPhPC DIB in hexadecane. (b) Voltage-induced thinning of a CSI in a 1 : 1 (v : v) hexadecane : AR20 mixture. Droplet diameters are *ca.* 700–800 μm.

accompany the increase in interface capacitance. The middle inset image shows that the droplets are clearly connected, sharing a large planar interface and a larger contact angle between droplets at a voltage of 200 mV. Finally, when the voltage is reduced to 0 mV, the capacitive current returns to its original amplitude and an image of the droplet pair shows that the droplets return to a separated state. This process is repeatable (see ESI† for video showing repeatable adhesion across multiple CSIs between electrodes); adhesion is regenerated by increasing the applied voltage to above 150 mV. Moreover, the area of adhesion between droplets can be reversibly varied (quantified in the next section) by modulating the applied voltage at a level greater than the minimum required to drive adhesion. In summary, the voltage activated CSI's are manipulatable and reversible.

Fig. 2 shows that this same type of fully reversible, voltage-induced adhesion between droplets is also obtained for triblock-coated droplets placed in *n*-decane, *n*-hexadecane, a 3 : 1 (v : v) hexadecane : AR20 mixture, and pure AR20 silicone oil, each containing the same concentration (4 mg mL^{-1}) of PEO-*b*-PDMS-*b*-PEO copolymer. By incrementally increasing voltage in 20 mV steps, we determine that the average minimum voltage, V_T, required to initiate adhesion between droplets is 166 mV (n = 5) in decane, 83 mV (n = 5) in hexadecane, 179 mV (n = 5) in 3 : 1 hexadecane : AR20 (n = 5), 371 mV (n = 5) in 1 : 1 hexadecane : AR20 (n = 5), and >1 V (n = 5) in pure AR20. Fig. 2 also lists the rupture potential (the voltage at which the interface ruptures causing the droplets to coalesce) for a DPhPC DIB and for CSIs assembled in each solvent. Similar to the threshold potential for adhesion, we observe that CSIs assembled in oil mixtures containing AR20 silicone oil display higher rupture potentials than those obtained in alkanes. Interestingly, a rupture potential was not reached for applied voltages up to 30 V (the limit of our power supply) for CSIs contained in pure AR20. Further, the rupture potential values for CSIs tested here are all significantly higher than that (212 mV, n = 7) found with DPhPC DIBs formed in hexadecane.

3.2 Quantitative characterization of voltage-induced CSIs

A lipid bilayer is commonly modeled as a resistor and capacitor wired in parallel.[49] Therefore, to better understand the structures of CSIs and to evaluate their barrier properties, we measured the squarewave current induced by the sum of a 10 mV, 10 Hz triangle wave voltage and a dc bias varied between the adhesion threshold and rupture potential. Values for nominal membrane capacitance and resistance at each bias level are extracted from the current traces using a custom MATLAB script as described elsewhere.[50,51] Fig. 3 shows an example set of capacitance and resistance data obtained from the induced squarewave current measured while also applying a sequentially step-wise increasing bias potential (Fig. 3a) across a CSI in hexadecane. Reflecting the behavior seen in Fig. 1b for separated droplets, we observe that membrane capacitance is negligible and membrane resistance is maximum (our fitting routine permits a maximum value of 1000 GΩ) until the bias reaches a value of approximately ~50 mV. However as applied potential exceeds V_T (t ~ 450 s in Fig. 3), nominal capacitance begins to increase and nominal resistance exhibits a sharp decrease to a value of *ca.* 40–50 GΩ. The changes in these electrical properties coincide with formation of a planar adhesive connection between the droplets. The data in Fig. 3 show that additional increases in the bias potential cause the capacitance and resistance to continue to rise and fall, respectively. Finally, we observe these parameters rebound to the values of C and R observed when $V = V_T$ as the droplets detach upon returning the bias to zero. Resistance does not return to a value of 1000 GΩ because of the non-linear nature of the fitting routine, which overestimates values of R prior to initial droplet adhesion.

These data pose interesting questions about the mechanism for changes in both capacitance and resistance as a function of the bias. Specifically, what causes the capacitance to increase: a change

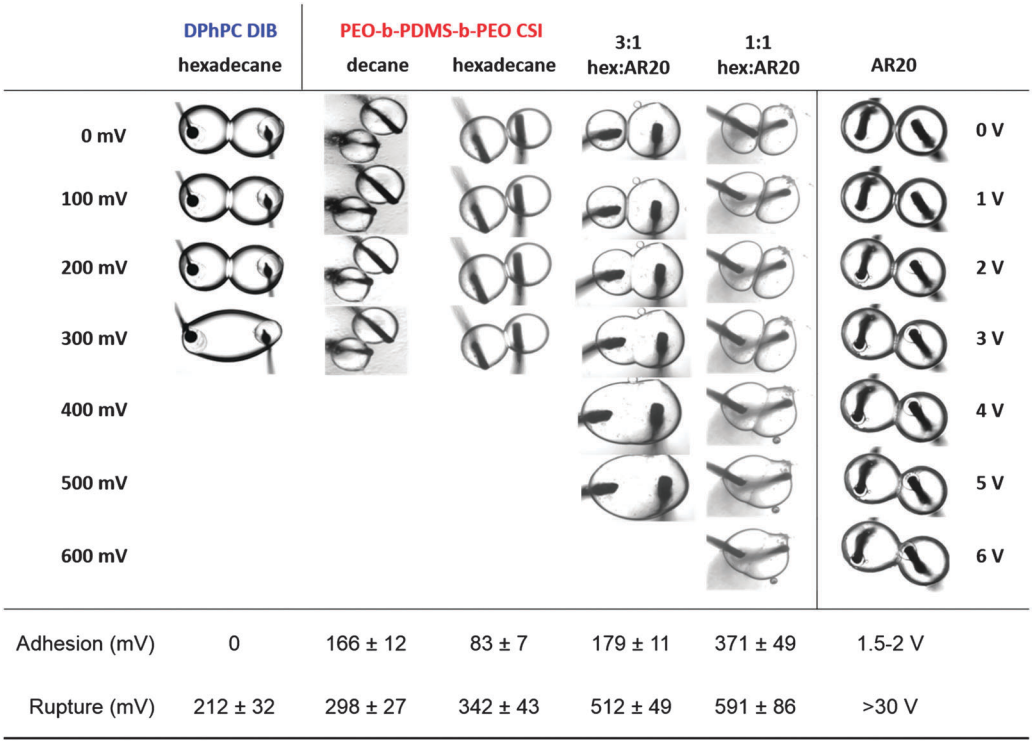

Fig. 2 DPhPC DIB *versus* voltage-induced CSI formation and rupture in different oils. Droplet diameters are *ca.* 700–800 μm (200 nL).

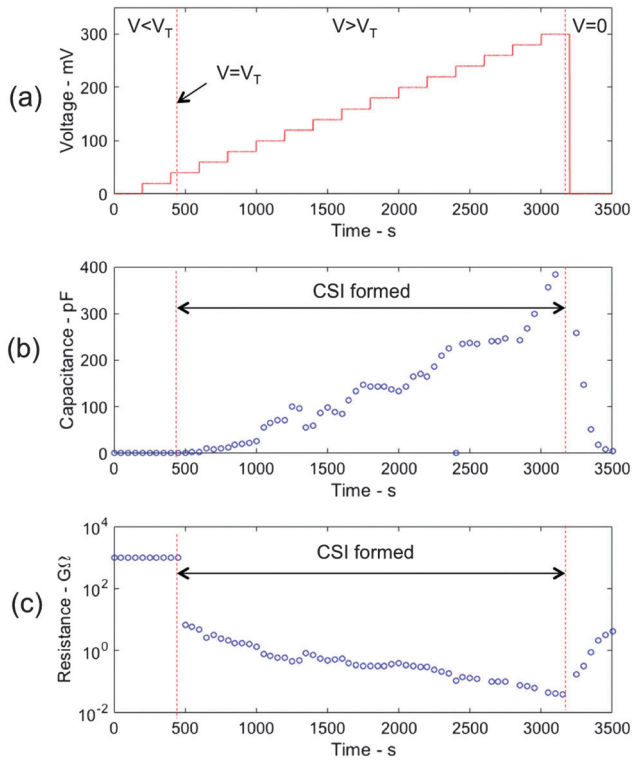

Fig. 3 (a) The applied bias voltage and (b) the resulting CSI membrane capacitance and (c) resistance.

in area of adhesion, or a decreasing interfacial thickness, or both? Also, does the reduction in membrane resistance correspond to a voltage-dependent leakage, or is this change driven solely by changes in membrane area? To answer these questions, we performed a separate set of experiments with gel-supported CSIs assembled using the droplet-on-hydrogel (DHB) method.[42,43,52] This approach allows us to accurately image the area of the interface while performing current measurements.

Fig. 4a shows the visual changes in the adhesive region underneath a gel-supported polymer coated droplet in decane when the voltage is increased from 0 mV to 300 mV; the arrows indicate the perimeter of the adhesive region (*i.e.*, the CSI). Note, the DHB method for CSI formation is utilized here due to the extremely low monolayer tensions of polymer-coated droplets in oil that complicates the calculation of bilayer area using images of adjacent, sagging droplets. Plotting the measured capacitance *versus* the square of the bias voltage (Fig. 4b) shows that the capacitance of the CSI exhibits a sharp increase at the threshold potential (~200 mV) and then increases linearly with respect to voltage squared. This trend is indicative of electrowetting behavior observed at a capacitive liquid interface as has been quantified for DIBs in recent publications.[41,42,53] For comparison, the voltage-dependent change in membrane capacitance for a DPhPC DIB (~30% increase) is provided in Fig. 4b to emphasize the much larger change (~400%) in membrane capacitance relative to nominal capacitance measured at V_T observed for the CSI. Repeating this experiment for CSIs in different oils shows that normalized membrane capacitance (relative to capacitance at V_T) varies linearly with respect to the square of the voltage difference between the bias potential and the threshold potential for that oil type (Fig. 4c). The slopes of

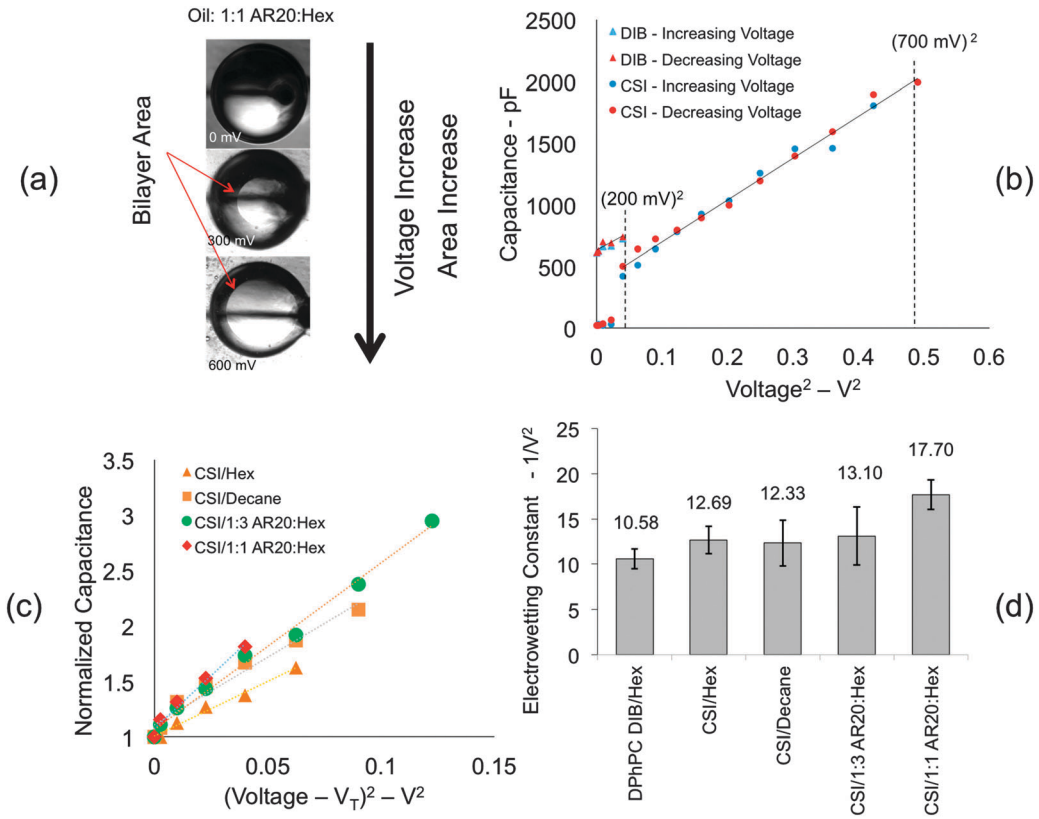

Fig. 4 (a) A gel-supported CSI in 1 : 1 AR20 : hexadecane shows the visible growth in adhesive area due to voltage. (b) Nominal capacitance measured on a DPhPC DIB in hexadecane and a CSI in the same oil as (a) *versus* the square of the applied bias. (c) Normalized capacitance *versus* change in voltage squared, and (d) the mean electrowetting constant after formation of the membrane for both a DPhPC DIB in hexadecane and CSIs in different oils.

the curves for each oil type in Fig. 4c represent the electrowetting constant, α, which describes the voltage-sensitivity of a capacitive interface. The bar graph in Fig. 4d compares the average values of electrowetting coefficient for CSIs formed in different oils (n = 3 in each oil) to that for DPhPC DIBs formed in hexadecane. All values range from 10–20 V^{-2}, and the data show that the strength of CSI electrowetting increases with the fraction of silicone oil in the nonpolar solvent surrounding droplets.

Fig. 5a shows the steady-state capacitance determined from the squarewave current magnitude, plotted *versus* the optically measured interfacial area of a CSI formed in 1 : 1 hexadecane : AR20. Unlike lipid-based DHBs which enable control of membrane area by changing the vertical position of the droplet,[42,43,54] these data reflect variations in membrane area caused by changing the applied bias voltage. Attempts to lift droplets with an electrode resulted in the droplets falling from the probe due to the low surface tension of copolymer-encased droplets. Yet, similar to a DIB,[41,42] we find that nominal capacitance varies linearly with interfacial area. The slope of the capacitance–area curve, which for this oil type has a value of 0.126 μF cm^{-2}, represents the specific capacitance, C_m, as given by:

$$C_m = \frac{C}{A} = \frac{\varepsilon_r \varepsilon_0}{t}, \quad (1)$$

where ε_r is the relative permittivity of the hydrophobic region of the membrane, ε_0 is the dielectric permittivity of vacuum (8.85×10^{-12} F m^{-1}), and t is the hydrophobic thickness of the membrane. Linear relationships between nominal capacitance and interface area are also found for the other oils (not shown; C_m cannot be determined in pure silicone oil due to the voltage limit of our current measurement device). The linearity of these data indicate that for $V > V_T$, voltage-driven increases in CSI capacitance are explained fully by increases in interfacial area at constant hydrophobic thickness (*i.e.* C_m is not voltage dependent). As shown in Fig. 4, these electrowetting-driven increases in membrane area range from 150–400% for CSIs, which is considerably higher than what we observe for a DPhPC lipid bilayer in hexadecane (~30%). Fig. 5b compares the average values of C_m measured for CSIs in various oils. Compared to a DPhPC DIB in hexadecane, CSIs exhibit much lower values of C_m. Moreover, we observe that CSIs formed in oils containing silicone oil exhibit slightly lower values of C_m than those formed in alkanes.

The hydrophobic thickness for each CSI is determined from these values of C_m using eqn (1) and is shown in Fig. 5c. The calculation is performed by using a value of ε_r = 2.6 to describe the dielectric properties of the triblock copolymer interface hydrophobic region (ε_r for PDMS ranges from 2.3–2.8[55,56]). It is noted that thinned CSIs may contain some residual amount of solvent as with lipid bilayers,[57,58] and the relative permittivity of alkanes like decane and hexadecane tends to be closer to 2.2,[59] thus our approximation may slightly overestimate hydrophobic

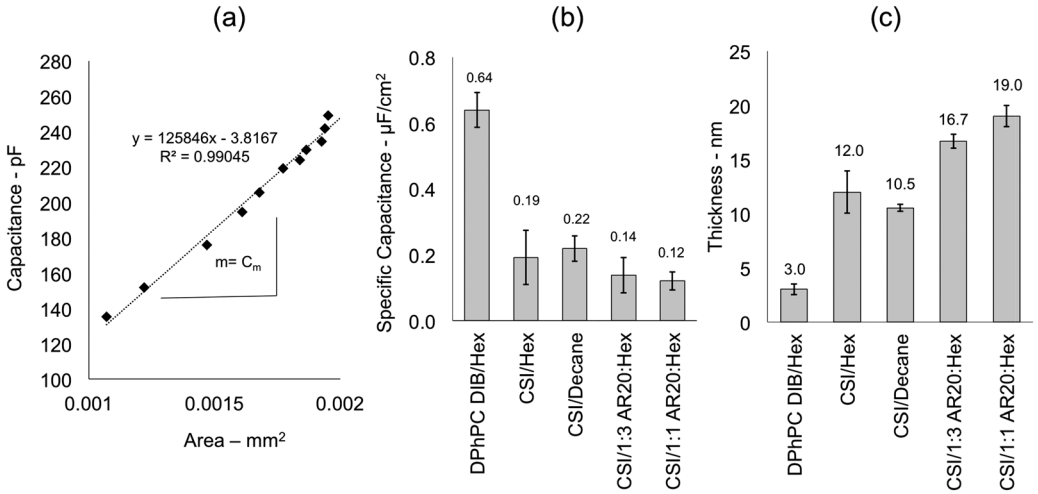

Fig. 5 (a) Representative nominal capacitance *versus* adhesive area data obtained for a CSI formed in 1 : 1 AR20 : hexadecane. This type of data for each interface allows calculation of the average specific capacitance (b) and equivalent membrane thickness (c).

thicknesses (especially in cases where pure alkanes are used, since AR20 and PDMS are expected to both have a dielectric permittivity of $\sim$2.6). Nonetheless, these calculations show (Fig. 5b) that the reduction in C_m for CSIs compared to a DIB (ε_r = 2.2) is the result of the interface having a considerably thicker hydrophobic region (10–20 nm). These data also show that CSIs in alkanes are thinner than those in silicone oil mixtures, which suggests that CSIs formed in alkanes contain less residual solvent upon voltage-initiated adhesion. Measured thickness values also compare well to those predicted for polymer brushes with 100% surface coverage described by the Alexander–deGennes model[60]

$$L \approx Na. \quad (2)$$

Here L represents the height (or thickness) of the "brush," which in this case is comprised of the hydrophobic PDMS middle block extending into the oil, N is the number of PDMS segments, and a is the segment length. A 2 kDa PDMS block consists of approximately 28 repeat units; however we estimate N as being at most 14 segments in length to account for the fact that the copolymer likely resides in a looped configuration at the oil–water interface due to the ABA design of the triblock copolymer.[61,62] With a value of 0.6 nm for the segment length from literature,[63] L is estimated to be 8.4 nm. Therefore, a bilayer formed between co-polymer droplets displays a hydrophobic thickness on the order of $\sim$17 nm. These values (8.4 nm and 17 nm) represent the limiting situation where the PDMS chains of the membrane are laterally crowded such that they are maximally extended into the oil. In oils where PDMS is less soluble or chains less crowded, we expect the brush height and total membrane thickness to be reduced due to the fact that the PDMS blocks would prefer to reside in a more compact, less swollen state. The differences between the measured values of hydrophobic thickness and the predicted total membrane thickness may also be the result of inclusion of oil in the midplane, which can occur in planar lipid bilayers formed in oil.[64]

With values of thickness known for CSIs in different oils, we next computed the magnitudes of electric field required to initiate adhesion and cause rupture (Fig. 6a). These data are again compared to that for a DPhPC DIB, and we see that despite the higher rupture potentials for CSIs, the electric field required to rupture a DPhPC bilayer is approximately 2–3$\times$ higher than that which is required to cause rupture in the triblock-stabilized interfaces. Examination of the raw current measurements made on CSIs at voltages near the rupture potential (Fig. S2 in the ESI†) shows that the applied voltage causes transient increases in current shortly before an irreversible increase in current that coincides with membrane rupture and droplet coalescence. This observation, which we also observe in lipid bilayers, suggests the applied voltage causes electroporation of CSIs, which leads to membrane rupture.

Finally, values of membrane resistance ($R_m = R \times A$) are computed by multiplying the measured resistance of a CSI by its respective area (determined by dividing nominal capacitance by C_m) at every bias voltage (Fig. 6b). Despite CSIs exhibiting far lower values of nominal resistance (0.2–2 GΩ) than lipid bilayers (10–100 GΩ), values of CSI membrane resistance on the order of 20–30 MΩ cm^2 are quite similar in magnitude to those for lipid bilayers (10–100 MΩ cm^2). Additionally, we see that the membrane resistance of each CSI–oil combination is generally constant *versus* voltage, and thus interfacial area. As a result, we can interpret the decrease in nominal resistance observed in Fig. 3c as being due primarily to the increase in area, and not due to voltage-initiated permeation. The permeability of this type of membrane to species other than ions is still largely untested, however a preliminary experiment demonstrated that carboxyfluorescein does not diffuse through a CSI formed (with $V > V_T$) in a 1 : 1 mixture of hexadecane : AR20.

While the results described thus far show how voltage affects CSI thickness and interdroplet contact area, little is known about the organization of triblock molecules and thus the tension states for both monolayer and the adhesive interface of a CSI.

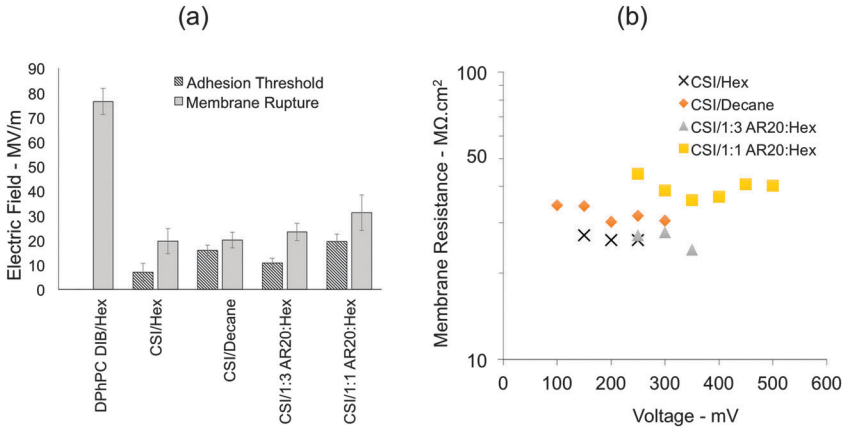

Fig. 6 (a) Computed electric field at both adhesion threshold and rupture voltages for a DPhPC DIB in hexadecane and for CSIs under different solvents. (b) Membrane resistance *versus* nominal voltage ($V > V_T$) of CSIs.

Knowledge of the monolayer and interfacial tensions of droplet-supported CSIs assembled in different oils would shed light on the mechanism for voltage-initiated adhesion, specifically pertaining to the role of solvent. Initially, we attempted to measure the monolayer tension of a triblock-covered water droplet in oil using a pendant drop goniometer. However, we observed the droplet to quickly sag in the less dense oil and then fall from the dispensing tip, which prevented us from being able to determine steady-state monolayer tension using the conventional pendant drop method.

Taylor *et al.* recently demonstrated that the steady-state monolayer tension of a DIB can be measured by tracking the electrowetting response of an interface for which C_m is known.[41] The method is based on the Lippmann relationship[65] which states that upon application of voltage across the capacitive bilayer interface, bilayer tension, γ_b, is reduced by the magnitude of the energy stored at the interface due to capacitive charging as given by

$$\gamma_{b,0} - \gamma_b(V) = \frac{C_m}{2}V^2, \quad (3)$$

where $\gamma_{b,0}$ is the bilayer tension at zero volts, C_m is the specific capacitance of the interface, and V is the applied voltage. For adhesive droplets that exhibit a planar interface and an external half contact angle, θ, γ_b is related to the monolayer tension, γ_m, *via* Young's relationship which is given by

$$\gamma_b = 2\gamma_m \cos\theta. \quad (4)$$

For a DIB that forms spontaneously at a zero bias, combining eqn (3) and (4) produces an expression that relates the change in the cosine of the contact angle to C_m, γ_m, and V. However, because CSIs exhibit electrowetting only at non-zero biases, eqn (3) and (4) are rewritten as

$$\cos\theta_{ref} - \cos\theta(V) = \frac{C_m}{4\gamma_m}\left(V^2 - {V_{ref}}^2\right) \quad (5)$$

to reflect how the cosine of the contact angle changes with respect to θ_{ref}, defined as the external contact angle measured at a non-zero reference bias V_{ref} located above the threshold potential.

Since C_m is known for the CSIs in various solvents, eqn (5) and (4), respectively can be used to determine unknown values of γ_m and γ_b by measuring the change in the cosine of θ *versus* the change in V^2. Therefore, a final series of experiments was performed on CSIs formed between adjacent droplets to investigate how the contact angle between droplets changes with the bias. Fig. 7a and b shows representative data for the measured change in the cosine of the contact angle *versus* $(V^2 - {V_{ref}}^2)$ for CSIs in each oil. The data are plotted on separate axes to account for the difference in scale between the values obtained for CSIs in alkanes *versus* those in silicone oil mixtures. All curves display a generally linear relationship between change in cosine of the contact angle and the difference in the square of the applied bias; R^2 correlation coefficient values for all curves are greater than 0.89, and greater than 0.96 for CSIs in silicone oil mixtures. In total, data were obtained from three separate interfaces formed for each CSI–oil combination. With eqn (5) and the corresponding average value of C_m for each CSI–oil (Fig. 5b), the slope of each linear regression is used to calculate γ_m. Fig. 7c compares the average monolayer tensions of CSIs to that measured on a DPhPC DIB. Interestingly, while the monolayer tensions for CSIs in alkanes are similar in magnitude to that for a DPhPC monolayer ($\sim$1–1.3 mN m^{-1} [46]), these data show that copolymer monolayers at a water–silicone oil mixture interface are considerably lower ($\sim$0.1 mN m^{-1}).

Average values for γ_b at V_T are computed for each CSI–oil case *via* Young's equation (eqn (4)). γ_m was computed for each in the previous section, and the contact angle, θ_t, measured at V_T is measured from images taken of adhered droplets after equilibration at V_T. Resulting values of θ_t and γ_b are shown in Fig. 7d and e for all CSIs and a DPhPC DIB. As observed with γ_m, these data again show that CSIs in alkanes exhibit membrane tensions ($\sim$2.0–2.5 mN m^{-1}) similar in magnitude to a lipid DIB, due to both similar values of monolayer tension and contact angle (20–30°). However, CSIs formed in silicone oil mixtures, those which display very low monolayer tensions, have substantially larger contact angles and thus even smaller

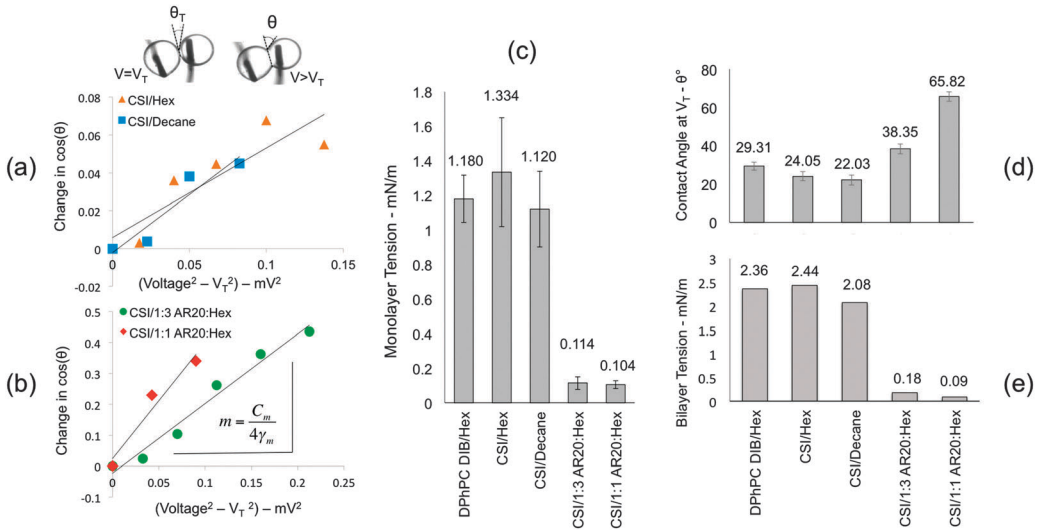

Fig. 7 The change in cosine of contact angle *versus* voltage squared for (a) CSIs in hexadecane and decane, and (b) for CSIs in 1 : 3 AR20 : Hex and 1 : 1 AR20 : Hex. (c) Monolayer tensions, (d) contact angles at the threshold voltage, and (e) computed average membrane tensions for a DPhPC DIB in hexadecane and for all CSIs.

relative membrane tensions (<0.2 mN m^{-1}). The Lippman (eqn (3)) and Young (eqn (4)) relationships predict that these interfaces reach an even lower tension, which corresponds to a higher contact angle, due to electrowetting at higher biases. This behavior is confirmed indirectly by the increasing contact angle observed with increasing voltage prior to rupture (Fig. 2). In fact, some of these interfaces approach an external half angle of 90°, which signifies the membrane reaches a zero-tension state.

These findings confirm why polymer-coated droplets consistently fell from the syringe tip during goniometer trials (extremely low γ_m), but they also reveal important differences about molecular packing at the interface. Specifically, the difference in tensions for CSIs in alkanes *versus* silicone oil mixtures suggest that copolymer molecules, likely in a looped configuration at the oil–water interface, are packed more tightly when the solvent contains silicone oil. Building on analysis by de Gennes,[66] we interpret the reduced tension and increased thicknesses of CSIs in silicone oil mixtures to confirm that the hydrophobic-PDMS middle block, which likely resides in a looped configuration at the oil–water interface, is extended from the interface but tightly packed in a lateral direction which serves to more effectively minimize the interfacial tension. In alkanes, our data suggest that the molecules are arranged in a more expanded state laterally, and they are also less swollen by solvent, which results in a shorter height—thus alkanes are relatively poorer solvents for PDMS expansion but still sufficiently good, which prevents spontaneous droplet adhesion. This behavior is not unexpected—"looped" polymer brushes arrayed at a solid–fluid interface remain stretched (swollen by solvent) and display repulsive intersurface interactions even when the solvent quality is worsened (to marginal, or θ-solvent conditions).[62] Fig. 8a shows a qualitative representation of these differences in molecular arrangement.

4 Discussion of the mechanism of reversible, voltage-initiated adhesion and CSI stability

Our experiments highlight key differences between the adhesion behavior and stability of DIBs and CSIs. DPhPC-coated droplets adhere spontaneously in hexadecane as well as in decane and silicone oil (not shown), confirming that these oils acts as poor solvents for the acyl chains of the DPhPC monolayers.[36] In a poor solvent, solvent is excluded due to unfavorable interactions, creating a solvent-depleted region of contact between droplets. This causes the area of the solvent-depleted region and the contact angle between droplets to scale inversely with tail solubility in the oil, which has been previously demonstrated: DPhPC DIBs formed in dodecane,[53] a smaller-molecule solvent in which the acyl chains have greater solubility, have a significantly smaller contact area compared to lipid-coated droplets connected in silicone oil.[67]

Like DIBs, polymer-coated droplets in alkane and silicone oil mixtures do not coalesce when placed in contact. However, unlike DIBs, they required a bias voltage to form an adhesive connection since the exclusion of oil is not favored, and they fully separate when this voltage is removed due to steric repulsion between opposing looped chains decorating the interface. The images and table in Fig. 2 highlight that the minimum voltage required to cause adhesion depends on the type of oil surrounding the droplets and that it increases for silicone-based oils *versus* pure alkane mixtures and with decreasing alkane length (*i.e.* decane *versus* hexadecane), a trend that is also observed in lipid bilayers.[68] This finding indicates that silicone oil is a better solvent than the two alkanes tested herein. In addition to the minimum voltage required to initiate adhesion, our knowledge of DIB area *versus* alkane length leads us to expect that the contact area of a voltage-thinned CSI at the threshold would scale inversely with solvent

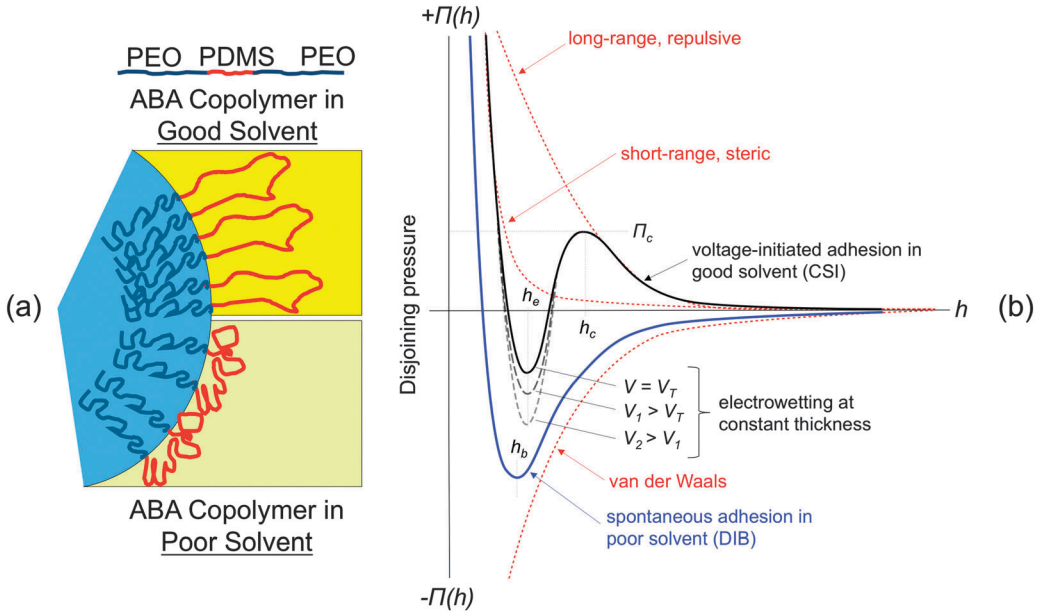

Fig. 8 (a) Illustration of conformations of copolymer molecules at the water–oil interface in good and poor solvents. (b) Qualitative disjoining pressure profiles *versus* separation distance for voltage-initiated CSI membranes formed in good solvents and DIBs assembled in poor solvents.

solubility. The images of CSIs in decane and hexadecane in Fig. 2 demonstrate this trend: CSI formation in decane, which appears to be a better solvent for PDMS, results in a smaller interfacial area at voltages above the threshold compared to the larger, more-easily excluded hexadecane. However, the fact that very low droplet surface tensions were obtained with solvents containing silicone oil allowed the droplets to assume a flattened, non-spherical shape. As a result, the images in Fig. 1 and 2 may not provide an accurate trend of relative bilayer size *versus* droplet radius for all oils tested. In a separate experiment, we studied the interactions of droplets coated with PEO-*b*-PDMS-*b*-PEO in a mixture of chloroform, hexadecane, and squalene at a volume ratio of 0.1 : 0.8 : 3.2. In this sufficiently poor solvent, we observed droplets to spontaneously adhere without voltage. The complete characterization of triblock interfaces formed spontaneously in poor solvents is currently ongoing.

Together, these findings confirm that the relative solubility of the hydrophobic copolymer middle block in an oil dictates the adhesion response of adjacent triblock-coated droplets. Our understanding of the mechanism of reversible, voltage-initiate adhesion for triblock polymer-coated droplets immersed in a good solvent is explained in the framework of the disjoining pressure. The disjoining pressure for reversible CSI formation in good solvent is illustrated qualitatively in Fig. 8b (black trace) as a function of separation distance, h, between two polymer-coated droplets, and this relationship is compared to that for spontaneous adhesion between surfactant-coated droplets in a poor solvent such as is observed with DIBs (blue trace).

As two droplets approach one another at large values of h, long-range repulsive interactions develop due to the presence of swollen polymer chains extending into the oil from each droplet surface. These interactions between polymer "brush" layers are entropic in nature and stem from a combination of osmotic repulsion interactions between solvated polymer coils which favors their expansion and the energy required to elastically stretch these chains.[60] The net effect is a repulsive barrier that prevents spontaneous adhesion. The application of voltage works to compress the thick interface and acts in opposition to these repulsive interactions, where the magnitude of the electrocompression[69] is given by

$$\Pi(h) = \frac{1}{2}\varepsilon_r\varepsilon_0\left(\frac{V}{h}\right)^2. \quad (6)$$

This applied pressure thins the interface through both elastic compression of the chains and through hydraulic exclusion of solvent from the interface. As applied voltage increases above zero but remains below the voltage threshold for adhesion, the system moves stably up the disjoining pressure curve (from right to left in Fig. 8b). A critical thickness is reached as soon as voltage reaches V_T, whereupon the interface spontaneously transitions to an adhesive interface like those shown in Fig. 1 and 2. This metastable point exists at a medium-range critical separation distance, denoted as h_c, where the electrocompressive forces cancel the long-range repulsive interactions, thereby thinning the interface, such that medium-range attractive van der Waals interactions between the two droplets now become the dominate forces balancing the system. This metastable balance point, denoted as Π_c thus represents the peak of the repulsive barrier before the two droplets transition spontaneously into an adhered state with an equilibrium thickness, h_e (Fig. 8b). The onset of adhesion is depicted as a reduction in the net disjoining pressure to a net negative value, and, importantly, is verified experimentally by the observed increase in contact angle between droplets when the voltage is increased above the threshold. Adhesion can be quantified by measuring or calculating the

reduction in free energy per unit area of the system upon the formation of the adjoining interface[68] as given by

$$-\Delta F(V) = 2\gamma_m - \gamma_b(V) = 2\gamma_m(1 - \cos\theta(\nu)). \quad (7)$$

Eqn (7) is written as a function of the applied voltage to emphasize that membrane tension is a function of applied voltage when electrowetting occurs. Once driven to an adhesive state, our measurements of C_m and thickness confirm that increasing the voltage further ($V > V_T$) only changes the area of the interface at constant thickness *via* electrowetting. The effect of electrowetting on the disjoining pressure is shown using dashed lines to illustrate the reduction in the local minimum at the equilibrium thickness, h_e.

In summary, applying voltage between polymer-coated droplets immersed in a sufficiently good solvent does work to overcome the positive disjoining pressure necessary for expelling solvent and compressing the interface. The interface thins stably as the voltage is increased up to a critical distance, h_c, at which spontaneous, attractive van der Waals interactions drive the droplets together to form an adhesive connection. Unlike recent reports of surfactant-coated droplets that coalesce under voltage,[69] the interfaces between copolymer-decorated droplets do not coalesce because the laterally overlapped monolayer of chains at the droplet interface results in repulsive steric interactions between opposing droplets. In the adhesive state, electrowetting merely causes the area of the interface to vary at constant thickness. Moreover, the process is reversible because the voltage-induced solvent expulsion establishes an osmotic pressure difference between the bulk oil and the interfacial hydrophobic region that favors driving solvent back into the membrane. Thus when the bias is reduced, the voltage-induced pressure lessens, and the compression-induced osmotic pressure causes oil to re-enter the membrane, whereupon chain swelling thickens the interface and pries apart the droplets. This behavior corresponds to traversing the disjoining pressure curve in reverse, where the osmotic pressure provides the work needed to overcome the peak. Hence, the use of voltage to drive adhesion for surfactant-coated droplets in a good solvent provides a mechanism for obtaining complete reversibility of contact between adjacent volumes.

The energetics of voltage-initiated adhesion can be quantitatively compared for CSIs in the various oils by calculating the critical disjoining pressure, Π_c, and the free energy of formation, ΔF. While the free energy of formation is related to the disjoining pressure profile, as given by

$$\Delta F = -\int_{\infty}^{h} \Pi(h)\mathrm{d}h, \quad (8)$$

our measurements of interfacial thickness *via* electrical capacitance are not sensitive to detecting changes in thickness greater than h_c (*i.e.* prior to droplet adhesion). Thus we are unable to convert values of ΔF into disjoining pressure units for the purposes of locating the minimum point in Fig. 8b. Additionally, we make the approximation that h_c and h_e are close in value since our measurement of thickness represents h_e. The results of these calculations are presented in Table 1.

Using the mean values of threshold voltage, monolayer tension, contact angle at the threshold voltage, we find that the critical disjoining pressure varies between ~1–4 kPa for CSIs, and it increases with increasing amounts of silicone oil in the solvent and increasing equilibrium thickness. This finding suggests that more pressure is required to exclude a silicone-oil-based organic phase due to the greater solubility of the PDMS block in AR20. This finding is supported by the increased thickness that we computed for thinned interfaces in silicone oil—suggesting that more oil remains even after repulsion is overcome with voltage. For the two alkanes, we see more pressure (and higher voltage) is required to exclude decane compared to hexadecane. This trend is consistent with lipid bilayers formed in alkanes, where smaller molecule solvents tend to be retained in the membrane more due to higher solubility. The inconsistency is the fact that despite a greater barrier to adhesion (suggesting higher solubility of decane in PDMS) our thickness data (Fig. 5c) does not indicate a statistically significant difference from that measured for CSIs in hexadecane, which has a lower adhesive barrier.

The values of free energy of formation per unit area reflect the decrease in free energy gained by adopting a planar interface with reduced tension between droplets. Larger external contact angles and lower membrane tensions thus correspond to a greater percentage reduction in free energy per membrane area compared to the energy per unit area (*i.e.* tension) of polymer monolayers prior to forming the adhesive interface. This calculation shows that CSIs formed in silicone oil exhibit a much larger relative decrease (20–60%) in energy per unit area than those formed in alkanes (~8%), as well as that for a DPhPC DIB in hexadecane (~6%).

Our experiments also show that voltage-initiated CSIs rupture at lower electric fields compared to their lipid bilayer counterparts (Fig. 6a). Examination of the raw current measurements for all CSI/oil combinations (Fig. S2 in ESI†) shows that these membranes become leaky prior to rupture—which we interpret as the formation of pores in the membrane that grow unstably. In thin films, pore formation is governed by the balance of the energy required to form new pore perimeter (characterized by an edge energy) *versus* the energy lost due to

Table 1 Energetics of DIB and voltage-initiated CSI formation

Oil type	V_T (mV)	θ_T (°)	Y_m (mN m^{-1})	h_e (nm)	$\Pi_c(h_e)$ (kPa)	$-\Delta F(h_e)$ (mJ m^{-2})	$\Delta F/2Y$ (% reduction)
CSI/Hex	83	24.1	1.32	0.19	1.20	0.23	8.1
CSI/decane	166	22.0	1.075	0.22	0.81	0.16	7.4
CSI/1 : 3 AR20 : Hex	179	38.4	0.114	0.14	2.42	0.05	21.9
CSI/1 : 1 AR20 : Hex	371	65.8	0.104	0.12	3.77	0.12	57.7

reduction in membrane area (characterized by a lateral membrane tension). This balance is a quadratic expression in terms of pore radius, and it can be modified[70–72] to include the contribution from an applied electric field, E, as given by:

$$\Delta W_p = 2\pi\Gamma r - \pi\gamma_b r^2 - \frac{1}{2}\left(\frac{\varepsilon_w}{\varepsilon_b} - 1\right)\varepsilon_b h E^2 \pi r^2, \qquad (9)$$

where ΔW_p is the change in energy required to form a pore of radius, r, Γ is the edge energy of the open pore, γ_b is the lateral tension of the bilayer, ε_w is the dielectric constant of water ($\sim$80), ε_b is the dielectric constant of the hydrophobic region of the membrane ($\sim$2), C_m is the specific capacitance of the membrane, and h is the thickness of the dielectric portion of the membrane. The final grouping of terms in eqn (9) describes the reduction in energy by substituting a charged region of membrane with a charged region of water that fills an open pore.[71] The critical pore radius is defined at the peak of this inverted parabola, a point at which a pore will grow spontaneously. The critical pore size and the energy required to get to this size thus define the barrier for stable *versus* unstable pores formed in membranes.

The difference in electric field required to drive rupture for DIBs and CSIs cannot simply be due to the difference in membrane tensions (Fig. 7e), since decreasing γ_b with respect to Γ favors a greater barrier to unstable pore formation. Further, we do not anticipate the slightly higher dielectric permittivity of a CSI membrane over a lipid bilayer to drive this reduction in electric field at rupture. Therefore, we conclude that both (1) a lower edge energy for pores in polymeric membranes compared to a pore in a lipid bilayer and (2) the higher thicknesses of CSIs cause pore formation that leads to rupture to occur at a lower electric field. Edge energy is related to the surfactant shape and the strength of surfactant–surfactant interactions. For example, it has been shown that short-chained (12 carbon), saturated PC lipids, which prefer to form micelles, exhibit lower edge energies compared to longer, saturated PCs.[70] In contrast, the high strength of lipid–lipid interactions of the bulky DPhPC acyl chains are known to increase the energy barrier to unstable pore formation. The fact that the PEG-*b*-PDMS-*b*-PEG macromolecules are considerably longer than lipids and reside in a looped configuration at the oil–water interface suggests that they may have greater flexibility that allows them to reduce the energy of a pore edge compared tightly packed DPhPC lipids. This reduction in order should decrease their ability to resist pore formation; thus we anticipate CSIs to exhibit lower Γ values compared to DPhPC membranes, favoring a lower electric field at rupture. In addition, our measurements proved that the dielectric thickness of CSIs ($\sim$10–20 nm) is 3–6$\times$ higher than that of DIBs ($\sim$3 nm). Both of these differences are responsible for the 2–3$\times$ lower electric field required to rupture a CSI compared to a DIB, and they are consistent with the fact that all CSIs (even ones with membrane tensions comparable to that for DPhPC DIBs) (Fig. 7e) rupture at considerably lower electric field values (Fig. 6a).

Unfortunately, we are unable to make the same comparisons regarding rupture conditions to CSIs formed in pure silicone oil. Due to constraints on our test hardware, we were able only to visually monitor adhesion for these interfaces, and were thus unable to estimate specific capacitance, thickness, and rupture voltage (and electric field). While charge screening in dielectrics is believed to limit the electrowetting response at high potentials,[73–75] we believe that CSIs formed in pure silicone oil are merely too thick to adequately charge or rupture. Based on measurements of CSIs formed in oils containing 25% and 50% AR20, we anticipate thin films formed in 100% AR20 to have thicknesses of $>$30 nm and specific capacitances of $<$0.001 μF cm^{-2}. According to eqn (3) and (5), lowering C_m lessens the change in the wetting angle for adhesive droplets. The images in the far right column in Fig. 2 confirm this; they show that little increase in interfacial area is observed as the voltage is increased beyond the threshold value for CSIs in pure silicone oil. The higher interfacial thickness also reduces the magnitude of the electric field at a given voltage, which prevented us from being able to reach the critical electric field level required to cause rupture.

5 Conclusions

To-date planar membranes assembled from triblock copolymer membranes have utilized a combination of good and poor solvents (typically chloroform—good and decane or toluene—poor) in proportions that leave the mixture predominantly poor for the middle hydrophobic block. This selection has resulted in the spontaneous membrane thinning.[12,13] In contrast, our study showed that polymer-stabilized adhesion between droplets in a sufficiently good solvent for the middle block is pressure-dependent and completely reversible, which indicates that there is an initial energy barrier to forming an adhesive interface. We quantified this barrier in the form the minimum applied pressure achieved *via* electrocompression needed to remove excess oil from between opposing monolayers. The results of these measurements show that the height of the repulsive barrier to adhesion increases with increasing solubility of the hydrophobic block in the oil; thus, more voltage or mechanical pressure is required to exclude solvent. Characterizations of the thinned interface upon overcoming the barrier to adhesion show that CSIs formed in silicone oil-based solvents yield thicker membranes that also exist at a lower tension state. These findings are supported by well known brush theories that predict an increase in brush length and a decrease in area per molecule at the interface for polymers in a good solvent. However, the demonstration of tuning this adhesion between small-volume droplets using voltage offers new capability for both connecting and disconnecting polymer-stabilized aqueous volumes, and enabling new forms of tunable modularity in droplet-based microfluidics, voltage-sensitive emulsions, and membrane-inspired material systems.

Acknowledgements

Nima Tamaddoni, Graham Taylor, and Stephen Sarles designed the experiments. Nima Tamaddoni, Graham Taylor, and Trevor Hepburn performed all experiments. Nima Tamaddoni, Graham Taylor, Michael Kilbey, and Stephen Sarles wrote the manuscript.

The authors acknowledge financial support from the Air Force Office of Scientific Research, Basic Research Initiative Grant Number FA9550-12-1-0464.

References

1 E. Reimhult and K. Kumar, *Trends Biotechnol.*, 2008, **26**, 82–89.
2 B. A. Heitz, J. Xu, I. W. Jones, J. P. Keogh, T. J. Comi, H. K. Hall, C. A. Aspinwall and S. S. Saavedra, *Langmuir*, 2011, **27**, 1882–1890.
3 S. Punnamaraju, H. You and A. J. Steckl, *Langmuir*, 2012, **28**, 7657–7664.
4 K. Dorn, R. Klingbiel, D. Specht, P. Tyminski, H. Ringsdorf and D. O'Brien, *J. Am. Chem. Soc.*, 1984, **106**, 1627–1633.
5 R. Benz, W. Prass and H. Ringsdorf, *Angew. Chem., Int. Ed. Engl.*, 1982, **21**, 869–880.
6 M. P. Cashion and T. E. Long, *Acc. Chem. Res.*, 2009, **42**, 1016–1025.
7 W. Meier, *Chem. Soc. Rev.*, 2000, **29**, 295–303.
8 H. Tanaka, M. Gomez, A. E. Tonelli and M. Thakur, *Macromolecules*, 1989, **22**, 1208–1215.
9 S. Okada, S. Peng, W. Spevak and D. Charych, *Acc. Chem. Res.*, 1998, **31**, 229–239.
10 C. Nardin, S. Thoeni, J. Widmer, M. Winterhalter and W. Meier, *Chem. Commun.*, 2000, 1433–1434.
11 W. Meier, A. Graff, A. Diederich and M. Winterhalter, *Phys. Chem. Chem. Phys.*, 2000, **2**, 4559–4562.
12 D. Wong, T.-J. Jeon and J. Schmidt, *Nanotechnology*, 2006, **17**, 3710.
13 C. Nardin, M. Winterhalter and W. Meier, *Langmuir*, 2000, **16**, 7708–7712.
14 J. Kowal, X. Zhang, I. A. Dinu, C. G. Palivan and W. Meier, *ACS Macro Lett.*, 2014, **3**, 59–63.
15 A. Gonzalez-Perez, V. Castelletto, I. W. Hamley and P. Taboada, *Soft Matter*, 2011, **7**, 1129–1138.
16 D. Morton, S. Mortezaei, S. Yemenicioglu, M. J. Isaacman, I. C. Nova, J. H. Gundlach and L. Theogarajan, *J. Mater. Chem. B*, 2015, **3**, 5080–5086.
17 G. Srinivas, D. E. Discher and M. L. Klein, *Nat. Mater.*, 2004, **3**, 638–644.
18 N. P. Kamat, J. S. Katz and D. A. Hammer, *J. Phys. Chem. Lett.*, 2011, **2**, 1612–1623.
19 V. Percec, D. A. Wilson, P. Leowanawat, C. J. Wilson, A. D. Hughes, M. S. Kaucher, D. A. Hammer, D. H. Levine, A. J. Kim, F. S. Bates, K. P. Davis, T. P. Lodge, M. L. Klein, R. H. DeVane, E. Aqad, B. M. Rosen, A. O. Argintaru, M. J. Sienkowska, K. Rissanen, S. Nummelin and J. Ropponen, *Science*, 2010, **328**, 1009–1014.
20 Y.-x. Shen, P. O. Saboe, I. T. Sines, M. Erbakan and M. Kumar, *J. Membr. Sci.*, 2014, **454**, 359–381.
21 G. Srinivas, D. E. Discher and M. L. Klein, *Nano Lett.*, 2005, **5**, 2343–2349.
22 M. Kumar, M. Grzelakowski, J. Zilles, M. Clark and W. Meier, *Proc. Natl. Acad. Sci. U. S. A.*, 2007, **104**, 20719–20724.
23 F. Itel, A. Najer, C. G. Palivan and W. Meier, *Nano Lett.*, 2015, **15**, 3871–3878.
24 P. Mueller and D. O. Rudin, *Nature*, 1968, **217**, 713–719.
25 P. Mueller, D. O. Rudin, H. T. Tien and W. C. Wescott, *Circulation*, 1962, **26**, 1167–1171.
26 M. Montal and P. Mueller, *Proc. Natl. Acad. Sci. U. S. A.*, 1972, **69**, 3561–3566.
27 K. Funakoshi, H. Suzuki and S. Takeuchi, *Anal. Chem.*, 2006, **78**, 8169–8174.
28 M. A. Holden, D. Needham and H. Bayley, *J. Am. Chem. Soc.*, 2007, **129**, 8650–8655.
29 H. Bayley, B. Cronin, A. Heron, M. A. Holden, W. L. Hwang, R. Syeda, J. Thompson and M. Wallace, *Mol. BioSyst.*, 2008, **4**, 1191–1208.
30 T. Wauer, H. Gerlach, S. Mantri, J. Hill, H. Bayley and K. T. Sapra, *ACS Nano*, 2013, **8**, 771–779.
31 G. Villar, A. D. Graham and H. Bayley, *Science*, 2013, **340**, 48–52.
32 G. Maglia, A. J. Heron, W. L. Hwang, M. A. Holden, E. Mikhailova, Q. Li, S. Cheley and H. Bayley, *Nat. Nanotechnol.*, 2009, **4**, 437–440.
33 G. J. Taylor and S. A. Sarles, *Langmuir*, 2015, **31**, 325–337.
34 K. Astafyeva, W. Urbach, N. Garroum, N. Taulier and A. R. Thiam, *Langmuir*, 2015, **31**, 6791–6796.
35 P. Poulin, F. Nallet, B. Cabane and J. Bibette, *Phys. Rev. Lett.*, 1996, **77**, 3248.
36 P. Poulin and J. Bibette, *Langmuir*, 1998, **14**, 6341–6343.
37 E. Evans, *Colloids Surf.*, 1990, **43**, 327–347.
38 P. Poulin and J. Bibette, *Langmuir*, 1999, **15**, 4731–4739.
39 J. Bibette, F. L. Calderon and P. Poulin, *Rep. Prog. Phys.*, 1999, **62**, 969.
40 S. Asakura and F. Oosawa, *J. Chem. Phys.*, 1954, **22**, 1255–1256.
41 G. J. Taylor, G. A. Venkatesan, C. P. Collier and S. A. Sarles, *Soft Matter*, 2015, **11**, 7592–7605.
42 L. C. M. Gross, A. J. Heron, S. C. Baca and M. I. Wallace, *Langmuir*, 2011, **27**, 14335–14342.
43 J. R. Thompson, A. J. Heron, Y. Santoso and M. I. Wallace, *Nano Lett.*, 2007, **7**, 3875–3878.
44 A. J. Heron, J. R. Thompson, A. E. Mason and M. I. Wallace, *J. Am. Chem. Soc.*, 2007, **129**, 16042–16047.
45 W. L. Hwang, M. Chen, B. Cronin, M. A. Holden and H. Bayley, *J. Am. Chem. Soc.*, 2008, **130**, 5878–5879.
46 G. A. Venkatesan, J. Lee, A. B. Farimani, M. Heiranian, C. P. Collier, N. R. Aluru and S. A. Sarles, *Langmuir*, 2015, **31**, 12883–12893.
47 A. D. Edelstein, M. A. Tsuchida, N. Amodaj, H. Pinkard, R. D. Vale and N. Stuurman, *J. Biol. Methods*, 2014, **1**, e10.
48 G. Villar, A. J. Heron and H. Bayley, *Nat. Nanotechnol.*, 2011, **6**, 803–808.
49 B. Hille, *Ion channels of excitable membranes*, Sinauer, Sunderland, MA, 2001.
50 P. Mruetusatorn, G. Polizos, P. G. Datskos, G. Taylor, S. A. Sarles, J. B. Boreyko, D. G. Hayes and C. P. Collier, *Langmuir*, 2015, **31**, 4224–4231.
51 J. B. Boreyko, G. Polizos, P. G. Datskos, S. A. Sarles and C. P. Collier, *Proc. Natl. Acad. Sci. U. S. A.*, 2014, **111**, 7588–7593.

52 A. J. Heron, J. R. Thompson, B. Cronin, H. Bayley and M. I. Wallace, *J. Am. Chem. Soc.*, 2009, **131**, 1652–1653.
53 S. Punnamaraju and A. J. Steckl, *Langmuir*, 2010, **27**, 618–626.
54 L. C. M. Gross, O. K. Castell and M. I. Wallace, *Nano Lett.*, 2011, **11**, 3324–3328.
55 *Polymer Handbook*, ed. J. Brandrup, E. H. Immergut and E. A. Grulke, Wiley-Interscience, New York, 4th edn, 2003, vol. 2, p. 2336.
56 M. B. H. Othman, M. R. Ramli, L. Y. Tyng, Z. Ahmad and H. M. Akil, *Mater. Des.*, 2011, **32**, 3173–3182.
57 S. H. White, *Nature*, 1976, **262**, 421–422.
58 S. H. White, *Biophys. J.*, 1978, **23**, 337–347.
59 G. Valincius, F. Heinrich, R. Budvytyte, D. J. Vanderah, D. J. McGillivray, Y. Sokolov, J. E. Hall and M. Lösche, *Biophys. J.*, 2008, **95**, 4845–4861.
60 J. N. Israelachvili, *Intermolecular and Surface Forces*, Academic Press, Saint Louis, MO, USA, 3rd edn, 2011.
61 X. Wang, J. L. Davis, J. P. Hinestrosa, J. W. Mays and S. M. Kilbey, *Macromolecules*, 2014, **47**, 7138–7150.
62 J. Alonzo, J. W. Mays and S. M. Kilbey Ii, *Soft Matter*, 2009, **5**, 1897–1904.
63 G. Beaucage, S. Sukumaran, S. J. Clarson, M. S. Kent and D. W. Schaefer, *Macromolecules*, 1996, **29**, 8349–8356.
64 T. J. McIntosh, S. Simon and R. MacDonald, *Biochim. Biophys. Acta, Biomembr.*, 1980, **597**, 445–463.
65 J. Requena and D. A. Haydon, *J. Colloid Interface Sci.*, 1975, **51**, 315–327.
66 P. G. de Gennes, *Macromolecules*, 1980, **13**, 1069–1075.
67 A. R. Thiam, N. Bremond and J. Bibette, *Langmuir*, 2012, **28**, 6291–6298.
68 D. Needham and D. A. Haydon, *Biophys. J.*, 1983, **41**, 251–257.
69 Z. Liu, S. T. Chan, H. A. Faizi, R. C. Roberts and H. C. Shum, *Lab Chip*, 2015, **15**, 2018–2024.
70 I. Genco, A. Gliozzi, A. Relini, M. Robello and E. Scalas, *Biochim. Biophys. Acta, Biomembr.*, 1993, **1149**, 10–18.
71 J. C. Weaver and Y. A. Chizmadzhev, *Bioelectrochem. Bioenerg.*, 1996, **41**, 135–160.
72 A. R. Thiam, N. Bremond and J. r. m. Bibette, *Phys. Rev. Lett.*, 2011, **107**, 068301.
73 J. Liu, M. Wang, S. Chen and M. O. Robbins, *Phys. Rev. Lett.*, 2012, **108**, 216101.
74 C. Quilliet and B. Berge, *Curr. Opin. Colloid Interface Sci.*, 2001, **6**, 34–39.
75 S. Chevalliot, S. Kuiper and J. Heikenfeld, *J. Adhes. Sci. Technol.*, 2012, **26**, 1909–1930.

